

Compressed Sensing Shape Estimation of Star-shaped Objects in Fourier Imaging

Jong Chul Ye

Bio Imaging & Signal Processing Lab.
Korea Advanced Institute of Science & Technology (KAIST)
373-1 Guseong-dong Yuseong-gu, Daejeon 305-701, Korea
E-Mail: jong.ye@kaist.ac.kr, Tel: +82-42-869-4320, Fax: +82-42-869-4310

March 20, 2007

Abstract

Recent theory of compressed sensing informs us that near-exact recovery of an unknown *sparse* signal is possible from a very limited number of Fourier samples by solving a convex L_1 optimization problem. The main contribution of the present paper is a novel non-parametric shape estimation framework and a computational algorithm for binary star shape objects, whose radius functions belong to the space of bounded-variation functions. Specifically, in contrast with standard compressed sensing, the present approach involves directly reconstructing the shape boundary under sparsity constraint. This is done by converting the standard pixel based reconstruction approach into estimation of a non-parametric shape boundary on a wavelet basis. This results in an L_1 minimization under a *nonlinear* constraint, which makes the optimization problem nonconvex. We solve the problem by successive linearization and application of one-dimensional compressed sensing, which significantly reduces the number of sampling requirements as well as the computational burden. Fourier imaging simulation results demonstrate that high quality reconstruction can be quickly obtained from a very limited number of samples. Furthermore, the algorithm outperforms the standard compressed sensing reconstruction approach using the total variation norm.

Index Terms

nonparametric shape estimation, compressed sensing, Fourier imaging

SPL EDICS: SAS-STAT, IMD-MDSP

I. INTRODUCTION

Consider a Fourier imaging problem to reconstruct a circular homogenous target with a support D against a uniform background. Conventional approaches for such problems are usually based on an inverse Fourier transform to reconstruct the pixel values within a field of view (FOV). In these approaches, the minimum number of measurement data is determined by the Nyquist sampling theory. If the sampling positions are randomly distributed

and the domain D is a sparse subset of the set representing the FOV, the recent theory of compressed sensing (CS) informs us that we can reduce the required number of samples significantly and still obtain perfect reconstruction by solving a convex optimization problem [1], [2]. Moreover, the number of Fourier samples can be further reduced for a piecewise constant image by replacing the L_1 norm with the 2-D total variation (TV) norm [1]. However, intuition tells us that we can further reduce the Fourier samples. For example, the zero frequency of the Fourier transform contains all the information about the size of a circular object. Then, why do the standard Fourier or CS approaches require considerably more measurement samples ?

The answer to this puzzling question is that most of the standard Fourier or CS approaches focus on reconstructing pixel values or the expansion coefficients in some basis rather than reconstructing the boundary information directly. Hence, regardless of whether the object is a circle or a complicated irregular object, the total sampling requirement is similar as long as the number of non-zero coefficients in some basis are the same [1].

The main contribution of this paper is the presentation of a novel non-parametric shape estimation framework and a computational algorithm. This is an extension of our previous parametric shape estimation works [3], [4], [5] to the non-parametric regime using a general boundary model with bounded variations to include all practical shape boundaries with cusps and discontinuities. Since this class of signals decay in a manner similar to a power-law within a wavelet basis [6], the coordinate functions of the boundary can be compactly expanded in a wavelet basis; hence, the original linear inverse problem can be converted into a one-dimensional nonlinear inverse problem of estimating the expansion coefficients under a sparsity constraint. However, due to a *nonlinear* constraint, the problem becomes nonconvex. Successive linearization and one-dimensional CS reconstruction [1], [2] are employed for the proposed algorithm, which significantly reduces the number of sampling requirements and the computational burden.

In the case of a piecewise constant image, such objects can be recovered very well using the standard CS reconstruction using the 2-D TV norm. However, our algorithm provides important advantages over the standard CS using the TV norm. In particular, the resolution of the standard CS using the TV norm is grid dependent. Hence, in order to represent cusps, oblique lines, and sharp corners, the standard CS reconstruction requires very fine discretization, which makes the reconstruction computationally expensive and requires substantially more Fourier samples.

This paper applies the new algorithm to a Fourier imaging problem. Especially, we are mainly interested in recovering boundary of star-shaped objects centered at the origin. Extensive simulation results show that accurate recovery of the complicated boundaries is feasible even with a severely limited number of Fourier samples and our algorithm outperforms the standard CS approach using the TV norm.

Schmid et al [7] reported on complexity regularized shape estimation, which uses the minimum description length (MDL) principle for model order selection. Specifically, they employ a parametric boundary representation such as Fourier descriptors, and the optimal model order is selected by comparing quality measures from multiple

reconstructions with distinct model orders [7]. However, our approach is fundamentally different from [7] since our algorithm is non-parametric and the optimal model order is automatically selected using a simple thresholding scheme. Hence, the present approach is much simpler and more accurate.

II. NON-PARAMETRIC SHAPE ESTIMATION PROBLEM

Consider a real-valued image f consisting of a constant-valued 2-D object:

$$f(\mathbf{r}) = \begin{cases} f_1, & \mathbf{r} \in D \\ 0, & \mathbf{r} \in \mathbb{R}^2 \setminus D \end{cases} \quad (1)$$

The region D is unknown, whereas the intensity f_1 is known. As shown in Figure 1(a), the boundary $S = \partial D$ need not be continuously differentiable, and may have cusps and discontinuities. In a Fourier imaging problem, the measurements are samples of a 2-D Fourier transform:

$$g(\mathbf{k}) = \int_{-\infty}^{\infty} \int_{-\infty}^{\infty} f(\mathbf{r}) e^{-j2\pi\mathbf{k}\cdot\mathbf{r}} d\mathbf{r}, \quad \mathbf{k} \in \mathbb{R}^2. \quad (2)$$

Mathematically, a boundary S is a one-dimensional (1-D) manifold in \mathbb{R}^2 : i.e. $S \triangleq \{\mathbf{s}(t) : t \in I = [0, 1]\} \subset \mathbb{R}^2$, where I is a unit interval. As explained before, we are mainly interested in estimating a star shaped object centered at the origin. The representation of a star shaped object is then given by $\mathbf{s}(t) = h(t) [\cos(2\pi t) \quad \sin(2\pi t)]^T$, where $h(t)$ is an angle dependent radius function for $t \in [0, 1]$. We assume that the radius function $h(t)$ belongs to $\mathbf{BV}[0, 1]$ - the space of objects with bounded variations within the unit interval [6]. More specifically, the space $\mathbf{BV}[0, 1]$ is a collection of functions whose total variation norms on $[0, 1]$ are bounded: i.e. if $h(t) \in \mathbf{BV}[0, 1]$, we have [6]:

$$\|h\|_V = \lim_{h \rightarrow 0} \int_0^1 \frac{|h(t) - h(t-h)|}{|h|} dt < \infty. \quad (3)$$

This class of boundary is a more general representation of a boundary than the smooth boundary since it includes boundaries with cusps and discontinuities. Furthermore, the signal in this class decays in the manner of a power law within a wavelet basis [6]. More specifically, if $\mathcal{B} = \{b_n\}_{n \in \mathbb{N}}$ is an orthonormal wavelet basis such that the function $h(t)$ can be expanded as follows

$$h = \sum_{n=1}^{\infty} \langle h, b_n \rangle b_n = \sum_{n=1}^{\infty} \theta_n b_n, \quad (4)$$

then for all $h \in \mathbf{BV}[0, 1]$ we can show that $\theta_{(n)}$ decays in the manner of a power-law [6]: $|\theta_{(n)}| \leq C \cdot n^{-3/2}$, where $\theta_{(n)}$ is the n -th largest wavelet coefficient and C denotes a positive constant. This implies that the wavelet expansion coefficients decay very rapidly and the radius function $h(t)$ is *sparse* in a wavelet basis. By stacking the expansion coefficients, we have

$$\boldsymbol{\theta} = \{\theta_n\}_{n \in \mathbb{N}} = \{|\langle h, b_n \rangle|\}_{n \in \mathbb{N}}. \quad (5)$$

Consider the following generic measurement framework from K *noiseless* measurement data, $\mathbf{y} \triangleq \{y(\mathbf{k}_i)\}_{i=1}^K$, $\mathbf{y} = \mathbf{F}(\boldsymbol{\theta})$, where $\mathbf{F}(\boldsymbol{\theta})$ is the noiseless nonlinear mapping from the surface $\mathcal{S} = \mathcal{S}(\boldsymbol{\theta})$ to the Fourier measurement vector $\{g(\mathbf{k}_i)\}_{i=1}^K$. The problem of estimating $\boldsymbol{\theta}$ then leads to the nonlinear least squares problem. There are, however, several technical difficulties in solving the nonlinear least square estimation problem. First, even if the mapping from the pixel values to the Fourier measurements is linear in the original inverse problems, the mapping from $\boldsymbol{\theta}$ to the measurement $\mathbf{y} = \mathbf{F}(\boldsymbol{\theta})$ is severely nonlinear. Second, the unknown vector $\boldsymbol{\theta}$ is infinite dimensional whereas we only have a finite-dimensional observation vector \mathbf{y} . Hence, the problem is a severely underdetermined *nonlinear* inverse problem, and some kind of regularization is needed to obtain accurate reconstruction of the boundary. Our approach is to exploit the sparsity of $\boldsymbol{\theta}$ to regularize the solution.

III. MAIN RESULTS

Rapidly developing theory of compressed sensing (CS)[1], [2] addresses the following underdetermined inverse problem of sizes (K, N) with $K < N, N \rightarrow \infty$:

$$\mathbf{y} = \mathbf{A}\mathbf{x}, \quad \mathbf{A} \in \mathbb{C}^{K \times N}, \quad (6)$$

where \mathbf{y} is the K -dimensional measurement vector, and \mathbf{x} denotes the N dimensional unknown signal, respectively. It is well known that there exist infinitely numerous solutions for the underdetermined problem Eq. (6). However, if \mathbf{x} is sparse and assumes non-zero values only at M locations, then the situation is drastically different. In particular, consider the following computationally feasible convex optimization approach [1], [2]:

$$(P1) : \min_{\mathbf{x}} \|\mathbf{x}\|_1 \quad \text{subject to } \mathbf{y} = \mathbf{A}\mathbf{x} \quad (7)$$

where $\|\cdot\|_1$ denotes the L_1 norm. The remarkable discovery of CS theory is that if the matrix \mathbf{A} satisfies certain conditions, called CS1-CS3 in [2] or the uniform uncertainty principle [1], (P1) guarantees the exact recovery of \mathbf{x} . Furthermore, if the measurement is noisy, (P1) can be modified to incorporate the influence of noise power:

$$(P1_n) : \min_{\mathbf{x}} \|\mathbf{x}\|_1 \quad \text{subject to } \|\mathbf{y} - \mathbf{A}\mathbf{x}\|_2 \leq \epsilon \quad (8)$$

where $\|\cdot\|_2$ denotes the L_2 norm and ϵ is the noise power, respectively. For this case, the reconstruction is still stable and the estimation error is bounded by

$$\|\mathbf{x}^* - \hat{\mathbf{x}}\|_2 \leq C_1 \epsilon \quad (9)$$

where \mathbf{x}^* and $\hat{\mathbf{x}}$ denote the true unknown parameters and the estimate of \mathbf{x} from K measurements, respectively, and C_1 is some constant [1], [2].

The direct application of (P1) for our non-parametric shape estimation can be written as follows:

$$(NP1) : \min_{\boldsymbol{\theta}} \|\boldsymbol{\theta}\|_1 \quad \text{subject to } \mathbf{y} = \mathbf{F}(\boldsymbol{\theta}) . \quad (10)$$

The main technical issue in (NP1) is that the constraint is now *nonlinear* with respect to $\boldsymbol{\theta}$. Hence, the basic concept of the present nonparametric shape estimation approach is to successively linearize the nonlinear functional $\mathbf{F}(\boldsymbol{\theta})$ at the current estimate of the wavelet coefficients vector. Specifically, for the noiseless measurements, we have

$$\mathbf{y} = \mathbf{F}(\boldsymbol{\theta}^*) = \mathbf{F}(\boldsymbol{\theta}_n) + \mathbf{F}'(\boldsymbol{\theta}_n)(\boldsymbol{\theta}^* - \boldsymbol{\theta}_n) + o(\|\boldsymbol{\theta}^* - \boldsymbol{\theta}_n\|_2) \quad (11)$$

where $\mathbf{F}'(\boldsymbol{\theta}_n)$ denotes the Fréchet derivative of the nonlinear function $\mathbf{F}(\cdot)$ at $\boldsymbol{\theta}_n$, $\boldsymbol{\theta}^*$ denotes the true parameter, and $o(\cdot)$ is the “small o” notation. We further introduce the following notation:

$$\mathbf{r}_n = \mathbf{y} - \mathbf{F}(\boldsymbol{\theta}_n) + \mathbf{F}'(\boldsymbol{\theta}_n)\boldsymbol{\theta}_n \in \mathbb{C}^K, \quad \mathbf{A}_n = \mathbf{F}'(\boldsymbol{\theta}_n) \in \mathbb{C}^{K \times N}. \quad (12)$$

(NP1) can then be converted into a form of the standard CS:

$$(P1') : \min_{\mathbf{x}} \|\boldsymbol{\theta}\|_1 \quad \text{subject to} \quad \|\mathbf{r}_n - \mathbf{A}_n\boldsymbol{\theta}\|_2 \leq \epsilon_n \quad (13)$$

where ϵ_n is given by $\epsilon_n = o(\|\boldsymbol{\theta}^* - \boldsymbol{\theta}_n\|_2)$. We now have the following:

Proposition 1: Suppose the Fréchet derivative $\mathbf{F}'(\boldsymbol{\theta}_n) \in \mathbb{R}^{K \times N}$, $n = 1, 2, \dots$, satisfies the CS1-CS3 [2] or the uniform uncertainty principle [1]. For a given initial estimate $\boldsymbol{\theta}_0$, successive application of (P1') guarantees the n -th reconstruction error ζ_n bounded by

$$\zeta_n \triangleq \|\boldsymbol{\theta}^* - \boldsymbol{\theta}_n\|_2 \leq o(\|\boldsymbol{\theta}^* - \boldsymbol{\theta}_0\|_2), \quad n = 1, 2, \dots. \quad (14)$$

Proof: The theorem can be proven by an inductive argument. The base for the induction is the observation of the linearization error $\epsilon_0 = o(\|\boldsymbol{\theta}^* - \boldsymbol{\theta}_0\|_2)$ due to Eq. (11). Then, Eq. (9) gives us $\zeta_1 = \|\boldsymbol{\theta}^* - \boldsymbol{\theta}_1\|_2 \leq o(\|\boldsymbol{\theta}^* - \boldsymbol{\theta}_0\|_2)$. The induction step consists in showing that if $\zeta_k \leq o(\|\boldsymbol{\theta}^* - \boldsymbol{\theta}_0\|_2)$, then $\zeta_{k+1} \leq o(\|\boldsymbol{\theta}^* - \boldsymbol{\theta}_0\|_2)$. The induction step follows directly since the linearization noise from the Taylor expansion Eq. (11) at $\boldsymbol{\theta}_k$ is given by $\epsilon_k = o(\|\boldsymbol{\theta}^* - \boldsymbol{\theta}_k\|_2)$ and the reconstruction error from the standard CS results under noisy measurements, Eqs. (8) and (9), tell us $\zeta_{k+1} \leq C_1\epsilon_k \leq o(\|\boldsymbol{\theta}^* - \boldsymbol{\theta}_0\|_2)$. This concludes the proof. ■

Note that the new L_1 minimization problem (P1') is based on the assumption that there exists a Fréchet derivative of $\mathbf{F}(\boldsymbol{\theta})$ at $\boldsymbol{\theta}_n$ for $n = 1, 2, \dots$. To calculate this quantity, a *shape derivative* or *domain derivative* is needed, as was discussed in detail in our previous works on the parametric shape estimation problem [4]. More specifically, the (i, j) -th elements of the Fréchet derivative $\mathbf{F}'(\boldsymbol{\theta}_n)$ can be calculated by computing $\partial g(\mathbf{k}_i; \boldsymbol{\theta}) / \partial \theta_j$ at $\boldsymbol{\theta} = \boldsymbol{\theta}_n$ as follows [4]:

$$\left. \frac{\partial g(\mathbf{k})}{\partial \theta_j} \right|_{\boldsymbol{\theta}=\boldsymbol{\theta}_n} = f_1 \int_0^1 e^{-j2\pi h(t; \boldsymbol{\theta}_n)(k_x \cos(2\pi t) + k_y \sin(2\pi t))} b_j(t) h(t; \boldsymbol{\theta}_n) dt, \quad (15)$$

where $h(t; \boldsymbol{\theta}_n)$ denotes the radius function calculated using $\boldsymbol{\theta}_n$. The computation of Eq. (15) can be easily done using the 1-D quadrature rule.

IV. RECONSTRUCTION ALGORITHM

Compared to the standard CS with TV norm [1], the computational complexity of our algorithm is smaller. Furthermore, a variety of pursuit algorithms for 1-D signal estimation can be used [1], [2], [8]. This paper follows the iterative soft-thresholding method of Daubechies et al [8]. Here, $\theta(i)$ denotes the i -th elements of the vector $\boldsymbol{\theta}$.

- 1) Set $n = 0$. Initialize $\boldsymbol{\theta}_0$ using a circle.
- 2) Calculate quantities \mathbf{r}_n and \mathbf{A}_n using successive linearization at $\boldsymbol{\theta}_n$ as shown in Eq. (12).
- 3) Set $\boldsymbol{\theta}_n^{(0)} = \boldsymbol{\theta}_n$. For $l = 0, 1, \dots, N_{max}$, apply the following iterative soft-thresholding to solve (P1'):
 - a) $\boldsymbol{\theta}_n^{(l+1)} = \boldsymbol{\theta}_n^{(l)} + \alpha_l \mathbf{A}_n^H (\mathbf{r}_n - \mathbf{A}_n \boldsymbol{\theta}_n^{(l)})$, where α_l is an appropriate step size.
 - b) For all i , if $|\theta_n^{(l+1)}(i)| \leq \lambda$, then $\theta_n^{(l+1)}(i) = 0$. Otherwise, $\theta_n^{(l+1)}(i) = \theta_n^{(l+1)}(i) - \lambda \text{sign}(\theta_n^{(l+1)}(i))$.
- 4) Update $\boldsymbol{\theta}_{n+1} = \boldsymbol{\theta}_n^{(N_{max})}$.
- 5) If not converged, $n \leftarrow n + 1$ and go to Step 2.

Note that our algorithm is different from the original iterative soft-thresholding algorithm presented by Daubechies [8] in that in our approach the original problem (NP1) should be successively linearized as the estimate updates. If \mathbf{r}_n and \mathbf{A}_n were not updated for each n , the proposed algorithm would be identical to the original iterative soft-thresholding algorithm [8].

V. NUMERICAL RESULTS

In order to generate a 2-D star shaped object, we first chose the object *Blocks* from the Wavelab package [9], and scaled it by 0.5 and added one to generate a radius function $h(t)$. This yields the original radius function, as shown in Figure 1(b). The corresponding 2-D boundary of a star shaped object with the radius function is illustrated in Figure 1(a). Suppose K numbers of Fourier samples are taken randomly from the sampling positions $\mathbf{k}_i \in [-k_{max}/2, k_{max}/2] \times [-k_{max}/2, k_{max}/2]$ for $i = 1, \dots, K$, where k_{max} denotes the maximum spatial frequency. For $k_{max} = 25$, the proposed reconstruction results using various numbers of Fourier samples are illustrated in Figs. 2(a), and (b) for sample numbers of $K = 150$, and $K = 250$, respectively. Nearly perfect reconstruction of the boundary can be obtained with only 150 Fourier samples using the proposed algorithm. Here, the initial surface \mathcal{S}_0 is set to be the unit circle with radius $r_0 = 1$. In order to demonstrate that the proposed algorithm outperforms the standard CS using the TV norm, we have modified the *l1-Magic* software (<http://www.acm.caltech.edu/l1magic/>) to incorporate the random Fourier samples and performed the simulation using the same sampling points as for the proposed method. The boundary estimations after segmenting the standard CS reconstruction using the TV norm with $K = 150$, and $K = 250$ are shown in Figs. 2(c), and (d), respectively. Overall, significant improvements were observed using the proposed method over the standard CS using the 2-D TV norm.

In order to quantify the convergence behavior of the proposed algorithm, Figure 3(a) presents the normalized root-

mean square error (NRMSE) plots of the proposed algorithm with respect to the iteration number. The NRMSE of the n -th estimate θ_n is defined as $NRMSE(n) = \|\theta^* - \theta_n\|_2 / \sqrt{N}$, where N is the dimension of the parameter θ , and θ^* denotes the true parameter vector. For all the sample numbers, the NRMSE converges as iteration proceeds. In Figure 3(b), we present the NRMSE plots of reconstructions using the proposed algorithm and the standard CS using the TV norm with respect to various numbers of Fourier samples. Again, it is clearly seen that the proposed algorithm outperforms the standard CS using the TV norm especially when the number of Fourier samples are very limited.

As a final example, we applied the algorithm to the reconstruction of a 2-D boundary of a low resolution Rotavirus image reconstructed using cryo-electron microscopy [10](see Figs. 4(a)(b)). The low resolution map was generated with in-house reconstruction packages using Rota virus samples measured from actual experiments. Again, the slice boundary is scaled such that the maximum radius is 1.5. In this experiment, we compared various reconstruction basis functions such as Haar wavelets, Daubechies wavelet with an order of 5 for the same number of measurement data $K = 200$ at $k_{max} = 25$. As shown in Figs. 4(c),(d), we observe that the smoothness of the reconstructed boundary depends on the regularity of the basis. Even though the global shape are fully recovered using all choices of basis, the Daubechies wavelet with an order of 5 provided the best reconstruction.

VI. CONCLUSION

We have developed a novel non-parametric shape estimation algorithm for inverse problems using compressed sensing. The proposed algorithm converted the 2-D shape estimation problem into a 1-D estimation problem by successive linearization using shape derivatives. This significantly reduced the sampling requirements of the imaging problem as well as the computational complexity. Fourier imaging simulation results using star shaped objects demonstrate that high quality reconstructions could be quickly obtained from a very limited number of samples and the proposed algorithm outperformed standard compressed sensing using the TV norm.

ACKNOWLEDGEMENTS

This work was supported by the grant No. R01-2005-000-10035-0 from the Basic Research Program of the Korea Science & Engineering Foundation. The author would like to thank Sung Ho Tak at KAIST for providing assistance in conducting the simulation.

REFERENCES

- [1] E. Candes, J. Romberg, and T. Tao, "Robust uncertainty principles: Exact signal reconstruction from highly incomplete frequency information," *IEEE Trans. on Info. Theory*, vol. 52, no. 2, pp. 489–509, Feb. 2006.

- [2] D. L. Donoho, “Compressed sensing,” *IEEE Trans. on Information Theory*, vol. 52, no. 4, pp. 1289–1306, April 2006.
- [3] J. C. Ye, Y. Bresler, and P. Moulin, “Asymptotic global confidence regions in parametric shape estimation problems,” *IEEE Trans. on Information Theory, Special Issue on Information Theoretic Imaging*, no. 5, pp. 1881–1895, August 2000.
- [4] J. C. Ye, Y. Bresler, and P. Moulin, “Cramér-Rao bound of parametric shape estimation in inverse problems,” *IEEE Trans. on Image Processing*, vol. 12, no. 1, pp. 71–84, January 2003.
- [5] J. C. Ye, P. Moulin, and Y. Bresler, “Asymptotic global confidence regions for 3-D parametric shape estimation in inverse problems,” *IEEE Trans. on Image Processing*, vol. 15, no. 10, pp. 2904–2919, October 2006.
- [6] S. G. Mallat, *A Wavelet Tour of Signal Processing*. Elsevier, 1999.
- [7] N. Schmid, Y. Bresler, and P. Moulin, “Complexity regularized shape estimation from noisy Fourier data,” *Proc. of IEEE Int’l Conf. on Image Proc.*, vol. 2, 2002, pp. 453–456.
- [8] I. Daubechies, M. Debrise, and C. D. Mol, “An iterative thresholding algorithm for linear inverse problems with a sparsity constraint,” *Comm. Pure and Applied Math.*, vol. 57, pp. 1413–1541, 2004.
- [9] J. B. Buckheit and D. L. Donoho, “WaveLab and reproducible research,” *Wavelets and Statistics*, no. 103, pp. 55–82, 1995.
- [10] T. S. Baker, N. H. Olson, and S. D. Fuller, “Adding the third dimension to virus life cycles: Three-dimensional reconstruction of icosahedral viruses from cryo-electron micrographs,” *Microbiology and Molecular Biology Reviews*, vol. 63, no. 4, pp. 862–922, 1999.

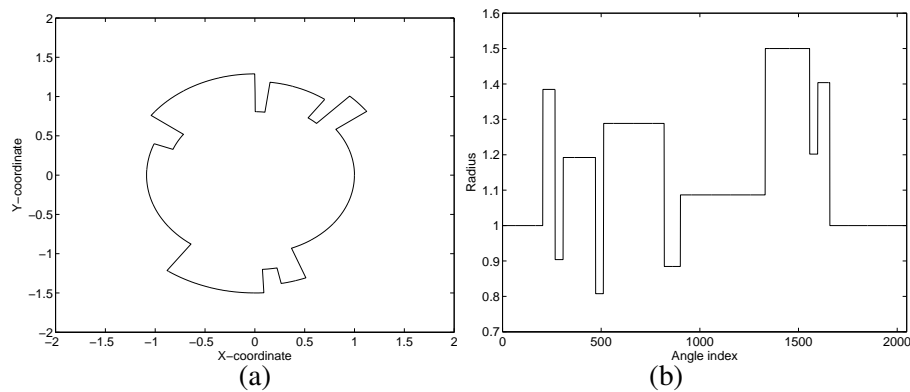


Fig. 1. (a) A star-shaped object, and (b) its corresponding radius function using *Blocks* functions in WaveLab [9].

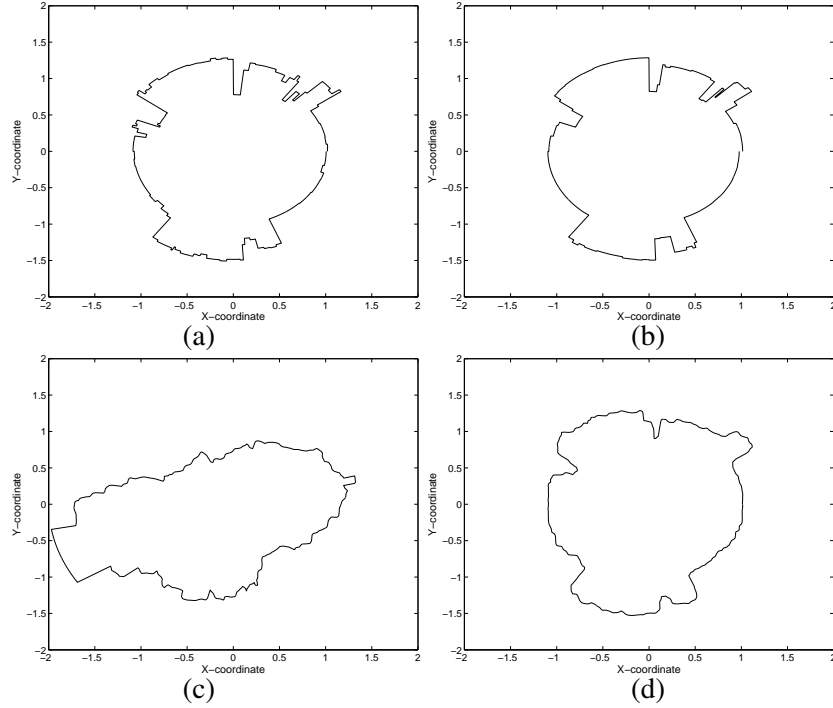


Fig. 2. (a)(b) Reconstruction of *Blocks* boundary using the proposed algorithm with various number of Fourier samples: $K = 150$, and $K = 250$, respectively. (c)(d) Standard CS reconstruction using TV norm with $K = 150$, and $K = 250$, respectively. The image and the frequency domain were discretized into 100×100 for the standard CS reconstruction using TV norm.

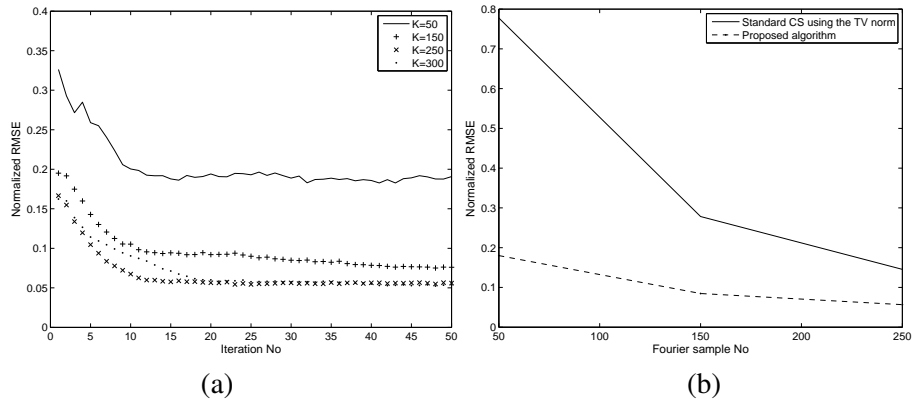


Fig. 3. (a) Convergence plots of the proposed algorithm with respect to the iteration, and (b) the comparison of the NRMSEs of the proposed algorithm and the standard CS using the TV norm.

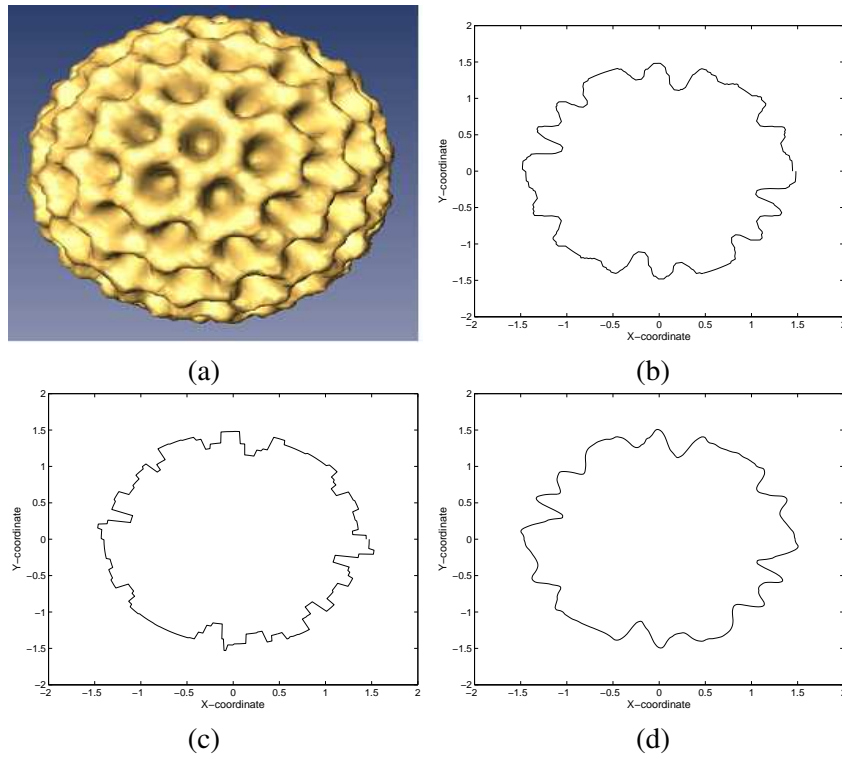


Fig. 4. (a) Low resolution Rota virus 3-D surface model, (b) a boundary of its central slice, (c) proposed reconstructions of Rota virus boundary using Haar wavelets, and (d) Daubechies wavelets of 5. All experiments were done at $k_{max} = 25$, $K = 200$ and $N = 512$.